Quantum Dot as a Resource for Teleportation and State Swapping

K.W. Choo[1] and L.C. Kwek[1,2]

[1]*Nanyang Technological University, National Institute of Education, 1, Nanyang Walk, Singapore 637616*
[2]*Department of Physics, National University of Singapore, 2 Science Drive 3, Singapore 117542*

(Dated: March 29, 2007)

We studied the use of the quantum dots as resource for teleportation and investigated how entanglement of the resource would affect the average fidelity of such process. We then identified suitable magnetic field, interdot distance and temperature to be used to achieve an average fidelity beyond the limit of classical communication channel. We also explored the effects of decoherence on the teleportation process. We then investigated the state transfer or swapping between two quantum dots. We found that perfect quantum swap is possible in this system. Smaller magnetic field and interdot distance shortened the perfect state transfer time. Finally we report on the performance of the system under different decoherence models.

PACS numbers:

I. INTRODUCTION

With dimensions ranging from a mere 1 nm to as much as 100 nm and consisting of anywhere between 10^3 to 10^6 atoms and electrons, semiconductor quantum dots are often regarded as artificial atoms. Charge carriers in a semiconductor quantum dot are confined in all three dimensions and the confinement can be achieved through electrical gating and/or etching techniques applied e.g. to a two-dimensional electron gas (2DEG).

For typical GaAs heterostructures the number of electrons in the quantum dots can be adjusted one by one starting from zero with typical magnetic fields, $B \approx 1$ T, corresponding to magnetic lengths on the order of $\ell \approx 10$ nm. This length is comparable to the size of the quantum dots. In this way, the dot spectrum depends strongly on the applied magnetic field. In coupled quantum dots which can be considered as artificial molecules, Coulomb blockade effects and magnetization have been observed as well as the formation of a delocalized "molecular state".

Entanglement between two quantum dots or qubits is achieved by coupling two spins, $\mathbf{S}_1$ and $\mathbf{S}_2$, temporarily through an exchange coupling $J(b,d)$ between them, described physically by a Heisenberg Hamiltonian,

$$H_s(b,d) = J(b,d)\mathbf{S}_1 \cdot \mathbf{S}_2. \tag{1}$$

Due to the Coulomb interaction and the Pauli exclusion principle the ground state of two coupled electrons is a spin singlet, i.e. a highly entangled spin state[? ?] . However recent experimental work on double quantum dots showed that if two electrons are in the sane quantum dot, they form a singlet. In the case of electrons in separated dots, the two electrons could occupy any spin state[?] . An appropriate pulsing of the exchanged coupling can correspond to a swap operator thereby creating an XOR gate[? ?] .

Assuming Heitler-London approach[? ?] , the exchange coupling can be written in the following form:

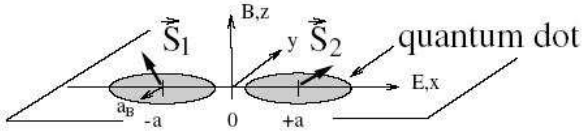

FIG. 1: Layout fo two coupled dots confined to the xy plan with spins $\mathbf{S}_1$ and $\mathbf{S}_2$.

$$J(b,d) = \frac{\hbar\omega_0}{\sinh\left(2d^2(2b-1/b)\right)}\left[c\sqrt{b}\left(e^{-bd^2}\mathrm{I}_0(bd^2) - e^{d^2(b-1/b)}\mathrm{I}_0(d^2(b-1/b))\right) + \frac{3}{4b}\left(1+bd^2\right)\right] \tag{2}$$

where $d = a/a_\mathrm{B}$ is the dimensionless distance, a is half the distance between the centers of the dots, and $a_\mathrm{B} = \sqrt{\hbar/m\omega_0}$ is the effective Bohr radius of a single isolated harmonic well. I_0 is the zeroth order Bessel function and $b = \omega/\omega_0 = \sqrt{1+\omega_\mathrm{L}^2/\omega_0^2}$, where $\omega_\mathrm{L} = eB/2mc$ denotes the Larmor frequency. The first and second terms in Eq. (**??**) are due to the Coulomb interaction C, where the exchange term enters with a minus sign. The parameter $c = \sqrt{\pi/2}(e^2/\kappa a_\mathrm{B})/\hbar\omega_0$ (≈ 2.4, for $\hbar\omega_0 = 3\,\mathrm{meV}$) is the ratio between Coulomb and confining energy. The last term comes from the confinement potential W. Fig. (**??**) depicts the layout of the two coupled quantum dots each confined to the xy plane, where the spins are denoted by $\mathbf{S}_1$ and $\mathbf{S}_2$ respectively.

II. ENTANGLEMENT OF FORMATION

In this section, we review entanglement measures. Entanglement is a mathematical quantity that measures the correlation between observable physical properties of a quantum system. Any function E that maps the state

space on positive real numbers satisfying the following requirements, can be used as entanglement measure:

1. $E(\rho)$ vanishes if the state ρ is separable.
2. E is invariant under local unitary transformations, i.e. local basis changes.
3. E does not increase on average under LOCC, i.e.

$$E(\rho) \geq \sum_i p_i E(\rho_i) \tag{3}$$

where in a LOCC the state ρ_i is obtained with probability p_i.

4. For pure state $|\psi\rangle$ the measure reduces to the entropy of entanglement,

$$E(|\psi\rangle\langle\psi|) = (S \circ tr_B)(|\psi\rangle\langle\psi|). \tag{4}$$

The entanglement of formation is defined by Wootters *et al*[?] . Given a density matrix ρ of a pair of quantum systems A and B, consider all possible pure-state decompositions of ρ, that is all ensembles of states $|\psi_i\rangle$ with probabilities p_i such that

$$\rho = \sum_i p_i |\psi_i\rangle\langle\psi_i|. \tag{5}$$

For each pure state, the entanglement E is defined as the entropy of either of the two subsystems A and B[?] :

$$E(\psi) = -\mathrm{Tr}\,(\rho_A \log_2 \rho_A) = -\mathrm{Tr}\,(\rho_B \log_2 \rho_B), \tag{6}$$

where ρ_A is the partial trace of $|\psi\rangle\langle\psi|$ over subsystem B, and ρ_B is defined similarly. The entanglement of formation of the mixed state ρ is then defined as the average entanglement of the pure states of the decomposition, minimized over all decompositions of ρ:

$$E(\rho) = \min \sum_i p_i E(\psi_i). \tag{7}$$

The basic Eq. (**??**) is justified by the physical interconvertibility of a collection of pairs in an arbitrary pure state $|\psi\rangle$ and a collection of pairs in the standard singlet state, the asymptotic conversion ratio being given by $E(\psi)$[?] . For a pair of qubits, the minimum value specified in Eq. (**??**) can be expressed as an explicit function of ρ. For ease of expression we will refer to the entanglement of formation simply as "the entanglement."

The formula for this entanglement makes use of what can be called the "spin flip" transformation, which is a function applicable both to state vectors and to density matrices of an arbitrary number of qubits. For a pure state of a single qubit, the spin flip, which is normally denoted by a tilde, is defined by:

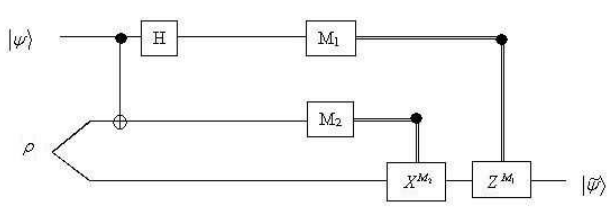

FIG. 2: Quantum circuit for teleporting a qubit. The two top lines represent Alice's system, while the bottom line is Bob's system. The double lines following the measurement M_1 and M_2 refer to classical channels for transporting classical bits.

$$|\tilde{\psi}\rangle = \sigma_y |\psi^*\rangle, \tag{8}$$

where $|\psi^*\rangle$ is the complex conjugate of $|\psi\rangle$ when it is expressed in a fixed basis such as $\{|\uparrow\rangle, |\downarrow\rangle\}$, and σ_y expressed in that same basis is the matrix

$$\begin{pmatrix} 0 & -i \\ i & 0 \end{pmatrix} \tag{9}$$

For a spin-$\frac{1}{2}$ particle, it is the standard time reversal operation that reverses the direction of the spin[?] . To perform a spin flip on n qubits, one can apply the above transformation to each individual qubit. If the system is described by a density matrix rather than a state vector, each σ_y is applied on both the right and the left sides of the matrix. For example, for a general state ρ of two qubits the spin-flipped state is given by:

$$\tilde{\rho} = (\sigma_y \otimes \sigma_y)\rho^*(\sigma_y \otimes \sigma_y), \tag{10}$$

where the complex conjugate is taken in the standard basis, which for a pair of spin-$\frac{1}{2}$ particles is $\{|\uparrow\uparrow\rangle, |\uparrow\downarrow\rangle, |\downarrow\uparrow\rangle, |\downarrow\downarrow\rangle\}$. In this case the spin flip is equivalent to "complex conjugation in the magic basis"[?] . Entanglement of formation of a mixed state ρ of two qubits is then given by:

$$E(\rho) = \mathcal{E}(C(\rho)), \tag{11}$$

where the function $C(\rho)$, or concurrence, is given by:

$$C(\rho) = \max\{0, \lambda_1 - \lambda_2 - \lambda_3 - \lambda_4\}, \tag{12}$$

where $\lambda_i, i = 1, \cdots, 4$, are the square roots of the eigenvalues of the product $\rho\tilde{\rho}$ arranged in decreasing order (i.e. $\lambda_1 > \lambda_2 > \lambda_3 > \lambda_4$).

III. QUANTUM DOTS AS A RESOURCE

Next, we look into the use of quantum dot described earlier as the resource for teleportation as shown in the

quantum network depicted by Fig. (**??**). We create quantum thermal states given in Eq. (**??**) as a resource ρ to be used for teleportation of an unknown state $|\psi\rangle$. The state ρ is given by:

$$\rho = \frac{e^{-\beta H}}{Z} \tag{13}$$

where H is the Hamiltonian, governed by Eg. (**??**), $Z = tr(e^{-\beta H})$ is the partition function, and $\beta = \frac{1}{kT}$ where k is Boltzmann's constant and T the temperature.

Let $|\tilde{\psi}\rangle$ be the output state of the teleportation process. we investigate the entanglement of formation $E(\rho)$ of the resource used, and how this entanglement would affect the average fidelity of the output states. We compute the average fidelity $\bar{F}$ using the following equation:

$$\bar{F} = \sum_{k=0}^{3} p_k \langle \psi_k | \tilde{\psi}_k | \psi_k \rangle \tag{14}$$

We then investigated the entanglement of formation of the resource $E(\rho)$ and the average fidelity of the output states ($\bar{F}$) under different magnetic field B, interdot distance d and temperature T, based on typical range of values proposed by Burkard *et al*[**?**] in their numerical analyses. We divided our investigations into two parts, in the first part, we investigate these effects under fixed interdot distance d, and in the second part, under the constant magnetic field B.

A. Fixed Interdot Distance $d = 0.2$

It has been shown[**?**] that the distance between the quantum dots affect the coupling between the dots, and increasing (decreasing) the interdot distance is physically equivalent to raising (lowering) the interdot barrier. It was observed[**?**] that the overlap of the wave function decays exponentially for large interdot distances $d \gg 1$ for $B = 0$ ($b = 1$). For small interdot distance, we choose $d = 0.2$ to investigate the entanglement of formation and the average fidelity of the system. We show in Fig. (**??**) the entanglement of formation of ρ, the mixed thermal state, generated for $1 < b < 2$ and $0 < T < 5$. Fig. (**??**) shows the average fidelity of the output states after the teleportation process. There is a very close correlation between the entanglement values of the resources and the average fidelities of the output states, i.e. the entanglement of the resource affect proportionally the fidelity of the teleportation process. We also observe that the average fidelity is close to 1 for $1 < b < 2$ and $T < 0.2$, and it decreases exponentially when T increases.

B. Fixed Magnetic Field $b = 1.2$

We next fixed the external magnetic field B such that $b = 1.2$ and investigated how the entanglement of the

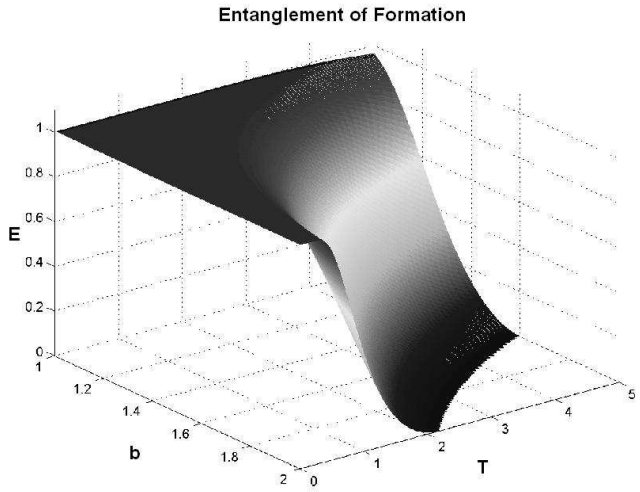

FIG. 3: Plot of Entanglement of Formation for $d = 0.2$

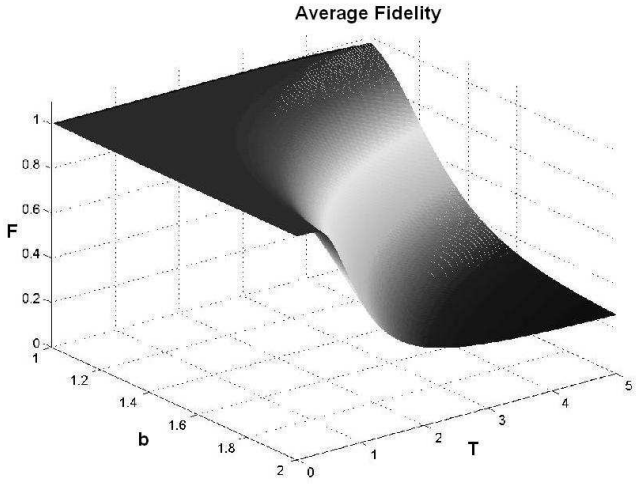

FIG. 4: Plot of Average Fidelity for $d = 0.2$

resources affect the average fidelity of the output states. Since $b = \omega/\omega_0 = \sqrt{1 + \omega_L^2/\omega_0^2}$, where $\omega_L = eB/2mc$ denotes the Larmor frequency, then minimum b value is unity when $B = 0$. For this simulation, the interdot distance varies between $0 < d < 1$ and temperature changes between $0 < T < 5$. The plots of entanglement and fidelity are shown in Fig. (**??**) and Fig. (**??**) respectively. In this case, the average fidelities maintain at unity for different temperature T when the interdot distance d is < 0.1. However, when d increases, the fidelity decreases exponentially, as does the entanglement. Again from these figures, we observed that the average fidelity of the output states is tightly correlated with the entanglement of formation of the resource states.

We then compare the performance of the system with classical ones knowing that the upper limit of the fidelity for a classical communication channel is $\frac{2}{3}$. It is expected that fidelity for a quantum channel should be better than

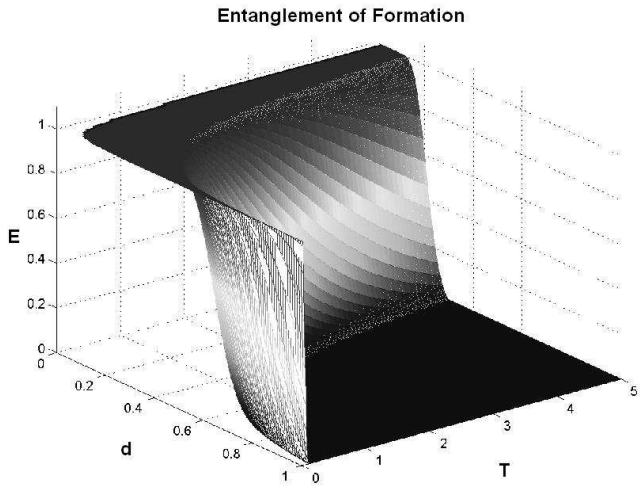

FIG. 5: Plot of Entanglement of Formation for $b = 1.2$.

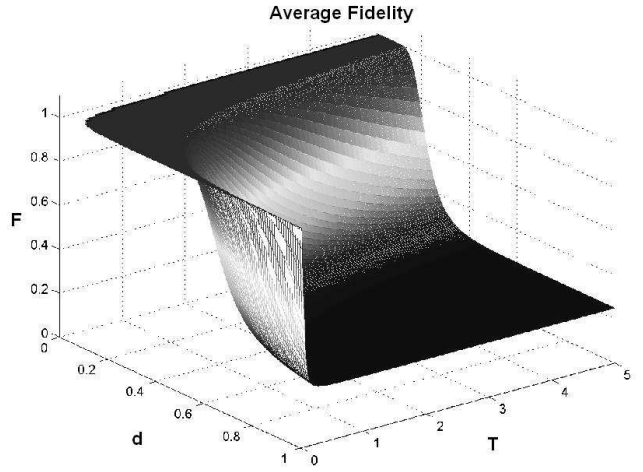

FIG. 6: Plot of Average Fidelity for $b = 1.2$.

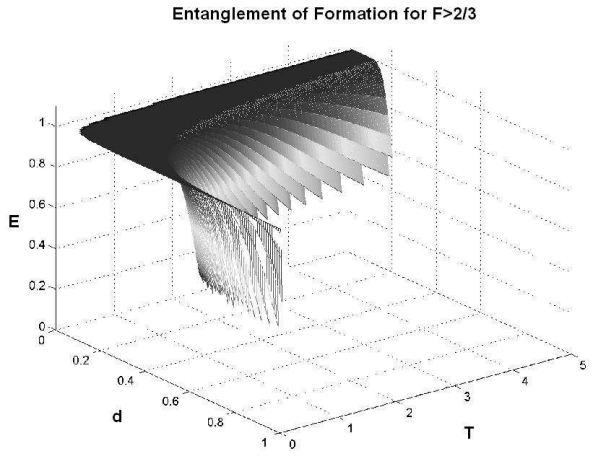

FIG. 7: Plot of Entanglement of Formation for $F > \frac{2}{3}$ with $b = 1.2$.

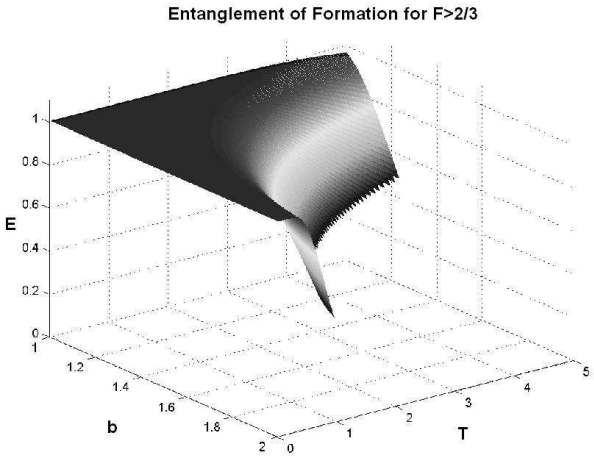

FIG. 8: Plot of Entanglement of Formation for $F > \frac{2}{3}$ with $d = 0.2$.

the classical case. We are interested to find out what entanglement values should the resource possess in order to achieve an average fidelity above the classical limit (of $\frac{2}{3}$) under different settings of B, d and T values. Fig. (**??**) shows the entanglement values of resources that can perform better than the fidelity of classical channel when magnetic field $b = 1.2$. Fig. (**??**) shows the entanglement values for resources that can perform better than the fidelity of classical channel at interdot distance $d = 0.2$.

The contour plots of the curve where $\bar{F} = 1$ and $\bar{F} = \frac{2}{3}$ are presented in Fig. (**??**) and Fig. (**??**). It is interesting to note that there is a small region (region A in Fig. (**??**) where the fidelity is guranteed to be unity. Fig. (**??**) also shows a region B in which the fidelity lies strictly between 2/3 and unity. Together both regions provide the values of d and T for a better than classical teleportation channel. Similarly Fig. (**??**) shows the contour plot for $\bar{F} = 1$ and $\bar{F} = \frac{2}{3}$ under variation of magnetic field b and T values. For the particular choice of interdot distance $d = 0.2$, the region corresponding to perfect fidelity is extremely small, and achievable only at very low temperature. The equivalent region for better than classical teleportation is labelled region C in Fig. (**??**).

C. Decoherence in Teleportation

For physical implementation of this system, one would require a good understanding of the effects of decoherence on the model. Decohenrece can be caused by interaction between the quantum state and its environment, causing dephasing or mixing with noise. In this study, we model typical decoherence under two different cases, namely the depolarizing channel and the dephasing channel. In the case of depolarizing channel, the decoherence is achieved by adding a noise admixture η into the quantum dot

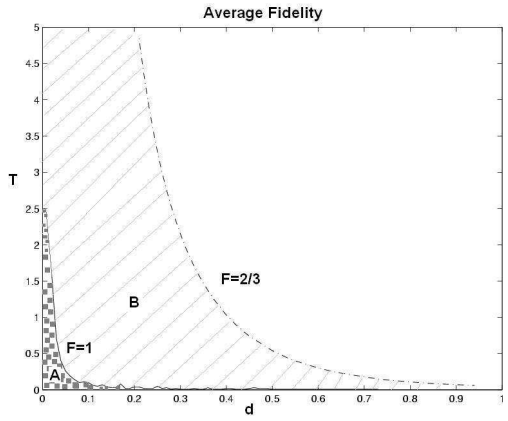

FIG. 9: Contour plot of average fidelity (corresponding to $F > \frac{2}{3}$) as a function of temperature T and interdot distance d with magnetic field $b = 1.2$.

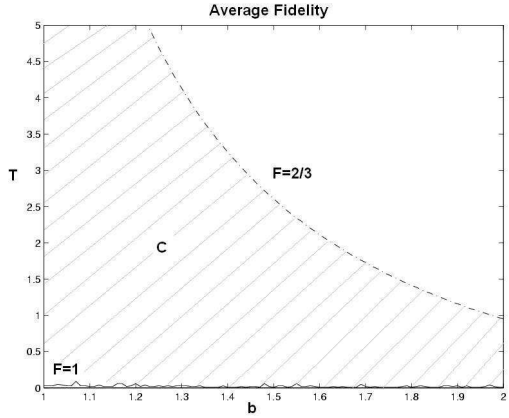

FIG. 10: Contour plot of average fidelity (corresponding to $F > \frac{2}{3}$) as a function of temperature T and magnetic field b with interdot distance $d = 0.2$.

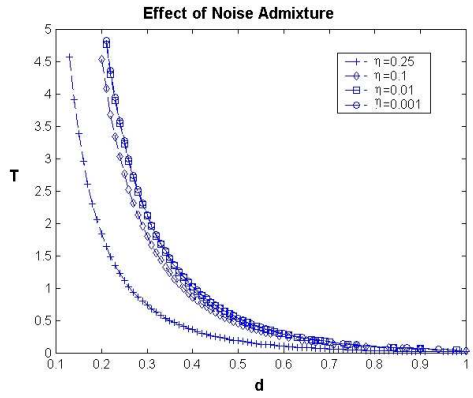

FIG. 11: Contour plot of critical average fidelity under depolarizing channel. This figure should be compared with Fig. (**??**) where the region under the critical average fidelity ($\bar{F} < \frac{2}{3}$) is smaller as η value increases.

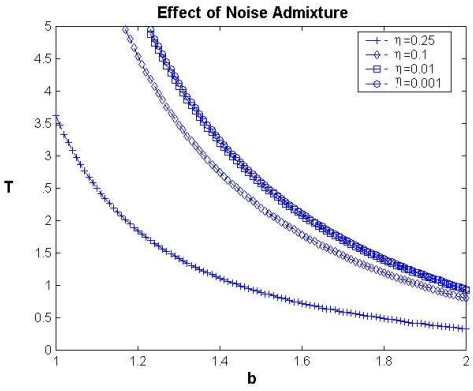

FIG. 12: Contour plot of critical average fidelity under depolarizing channel. This figure should be compared with Fig. (**??**). Similarly the region under the critical average fidelity ($\bar{F} < \frac{2}{3}$) is reduced under different η values.

system. Such a model effectively describes a decoherence system with bit flip and phase flip errors. The density matrix of the system under this type of decoherence is given by:

$$\rho(t) = (1-\eta)\rho(0) + \frac{\eta}{4} I_4. \tag{15}$$

Using Eq. (**??**), we investigate the effect of η on the teleportation process under different b, d and T values. Fig. (**??**) and Fig. (**??**) depict the situations under cases of fixed magnetic field ($b = 1.2$) and fixed interdot distance ($d = 0.2$) respectively. For contrast with the noiseless situation, these figures should be compared to Fig. (**??**) and Fig. (**??**) respectively. The region corresponding to an average fidelity of unity has in general vanished, i.e. the average fidelity under depolarizing channel is always less than unity. Moreover the region corresponding to $F > 2/3$ has also shrunk. However for moderate noise level,$\eta < 0.1$, the shrinkage may not be significant and could still be tolerable. Thus it may still be possible to perform teleportation in a depolarizing channel for a fairly wide range of temperature T, magnetic field b and interdot distance d under moderate noise level.

Another way to study the decoherence for the system is to consider a dephasing channel. In this paper, we refer to the general master equations of a qubit state. The most commonly used general master equation for a two-level system was given by Gorini *et al.*[?] and Lindblad[?] . Using the notation of Gorini *et al.* the master equation for the qubit density matrix can be written as:

$$\frac{\partial}{\partial t}\rho(t) = -i[H, \rho(t)] + \frac{1}{2}\sum_{i,j=1} \Gamma_{ij}[\sigma_i, \rho(t)\sigma_j] + [\sigma_i \rho(t), \sigma_j] \tag{16}$$

where H is a time-independent Hermitian operator represents the unitary component of the evolution. The second term is responsible for non-unitary processes such as decoherence, polarization and equilibration. The coeffi-

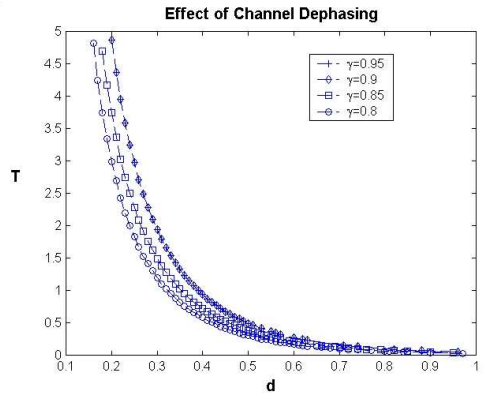

FIG. 13: Contour plot of critical average fidelity under the influence of dephasing channel. This figure should be compared with Fig. (**??**) where the region under the critical average fidelity ($\bar{F} < \frac{2}{3}$) is reduced when different channel dephasing γ values are introduced.

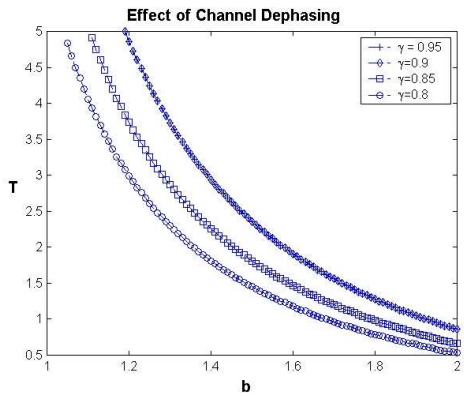

FIG. 14: Contour plot of critical average fidelity under the influence of dephasing channel. This figure should be compared with Fig. (**??**). Similarly the region under the critical average fidelity ($\bar{F} < \frac{2}{3}$) has shrunk under different channel dephasing γ values.

cients Γ_{ij} determine the decay or growth of polarization.

Using this master equation, we consider a dephasing model by Eberly *et al.*[?] , namely a two-qubit local dephasing channel ε_{AB} in which the pair of qubits interact via the local magnetic fields. The phase-noisy channel, denoted by ε_{AB}, is characterized by the following matrix:

$$\begin{aligned}\rho(t) &= \varepsilon_{AB}(\rho(0)) \\ &= \begin{pmatrix} \rho_{11} & \gamma_B\rho_{12} & \gamma_A\rho_{13} & \gamma_A\gamma_B\rho_{14} \\ \gamma_B\rho_{21} & \rho_{22} & \gamma_A\gamma_B\rho_{23} & \gamma_A\rho_{24} \\ \gamma_A\rho_{31} & \gamma_A\gamma_B\rho_{32} & \rho_{33} & \gamma_B\rho_{34} \\ \gamma_A\gamma_B\rho_{41} & \gamma_A\rho_{42} & \gamma_B\rho_{43} & \rho_{44} \end{pmatrix} \end{aligned} \quad (17)$$

where γ_A and γ_B are defined in Eq. (**??**) and the notation ρ_{ij} stands for the initial state $\rho_{ij}(0)$.

$$\gamma_A(t) \;=\; e^{-t/2T_2^A}, \;\; \gamma_B(t) = e^{-t/2T_2^B}, \qquad (18)$$

T_2^A and T_2^B are the phase relaxation times for qubit A and qubit B due to the interaction with their own environments. Dephasing channel could also be a useful model for studying decay in a quantum system. To simplify our studies, we assumed that the phase relaxation times for qubit A and qubit B are equal by choosing $\gamma = \gamma_A = \gamma_B$. Fig. (**??**) and Fig. (**??**) show the effects of dephasing channel on average fidelity of the system. In general, the effect on the quantum teleportation system is found to be similar to the depolarizing channel case. The average fidelity is always less than unity and the region where $\bar{F} > \frac{2}{3}$ shrunk as γ is increased. By comparing Fig. (**??**) and Fig. (**??**), we note that there is a greater change in the critical temperature corresponding to an average fidelity $\bar{F}$ of $\frac{2}{3}$ for a fixed magnetic field than an interdot distance.

IV. STATE TRANSFER OR SWAPPING

We also considered the use of coupled quantum dots for quantum state transfer or swapping. This ability to transfer a quantum state from one site to another is important in quantum information processing.

There are examples of quantum computing applications that use trapped atoms or photons in cavity QED[?] and phonons in ion traps[?] as information carriers to transfer states from one site to another. Recently, it has been shown in[? ?] that perfect state transfer is possible across a network of qubits, allowing only control over the initial design of the network, with no dynamical control required.

In our work, we showed that a perfect state transfer is also possible using Heisenberg Hamiltonian Eq. (**??**) and the Heitler-London approach Eq. (**??**). We set one of the quantum dots $\mathbf{S}_1$ as arbitraty state of $|\psi\rangle = \alpha|0\rangle + \beta|1\rangle$ and the other $\mathbf{S}_2$ as $|0\rangle$. The quantum system is allowed to evolve with time t following the mechanics of e^{-iHt}. At time t, the quantum dot system is governed by the following equation:

$$|\psi(t)\rangle = e^{-iHt}(|\psi\rangle|0\rangle). \qquad (19)$$

We want to find a time t at which the transfer fidelity is unity, signifying perfect state swapping, or a perfect state transfer. The transfer fidelity is computed from inner product of the reduced density matrix $|\rho_t^{red}\rangle$ at time t and the initial state $|\psi\rangle$. The reduced density matrix is computed from the density matrix of $|\psi(t)\rangle$, by tracing out the first qubit from it. Fig. (**??**) shows the plot of transfer fidelity F with time t. In this case, we have set the interdot distance to be 0.2 and magnetic field to $b = 1.2$ (these are the same settings used in the previous simulation). It is observed that the perfect state transfer is possible in the time interval of $0 < t < 1$ at t_0 and t_1 as shown.

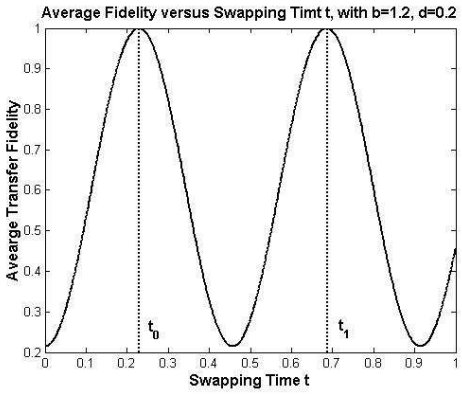

FIG. 15: Plot of Transfer Fidelity Versus Time ($b = 1.2$ with $d = 0.2$).

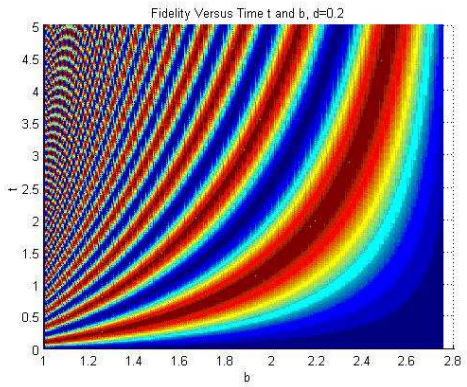

FIG. 17: Contour Plot of Transfer Fidelity Versus Time and Magnetic Field ($d = 0.2$).

$$F = \langle\psi|\rho_t^{red}|\psi\rangle \tag{20}$$

A. Fixed Interdot Distance with $d = 0.2$

In Fig. (**??**), we varied b under a fixed interdot distance of 0.2 and noticed that the fidelity oscilates between 0 and 1 as time evolves. In particular there may exist an optimum shortest time for perfect state transfer, in which the transferred (final) state at the second site is exactly the same as the initial state at the first site for sufficiently small b. Fig. (**??**) shows the contour plot of the transfer fidelity. We observed that as one reduces b, there is a decrease in the optimum shortest time for perfect state transfer. Moreover, the number of the occurrence for perfect state transfer increases. However, for large b, this optimum time increase exponentially. Fig. (**??**) shows the plot of optimum shortest time versus the choice of magnetic field.

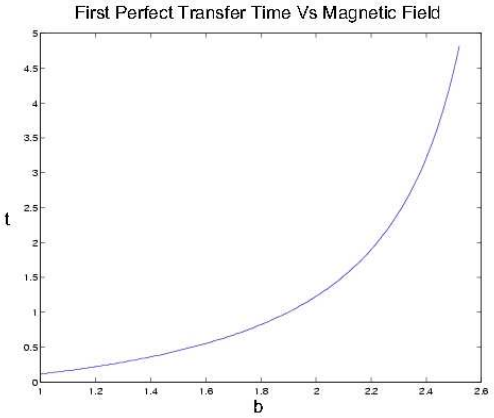

FIG. 18: Plot of time taken for first (optimum shortest) perfect transfer where fidelity $F = 1$. We observed that the optimum shortest time is longer as b increases, indicating that the swapping between the quantum dots $\mathbf{S}_1$ and $\mathbf{S}_2$ is slower under stronger external magnetic field.

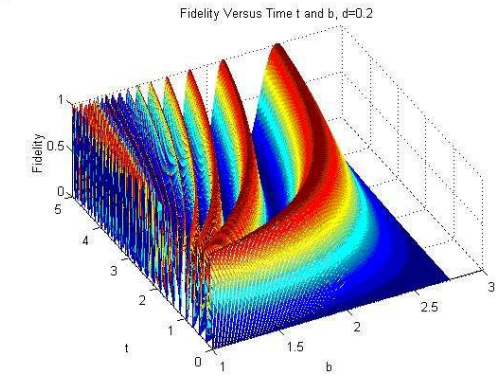

FIG. 16: Plot of Transfer Fidelity Versus Time and Magnetic Field ($d = 0.2$).

B. Fixed Magnetic Field with $b = 1.2$

We then investigated the influence of interdot distance d over the perfect state transfer time under constant external magnetic field. A similar profile was found and the result is plotted in Fig. (**??**). The contour plot of the fidelity is shown in Fig. (**??**) and we observed here that the number of occurrence for perfect state transfer is higher for for smaller interdor distance. Fig. (**??**) shows the changes in the optimum shortest time with respect to interdot distance d, where smaller d values contribute to shorter optimum transfer times. It is interesting to note that for larger interdot distance $d > 1$ where d is defined as a/a_B, the perfect state transfer optimum time increases quickly when a is greater that a_B (the effective Bohr radius).

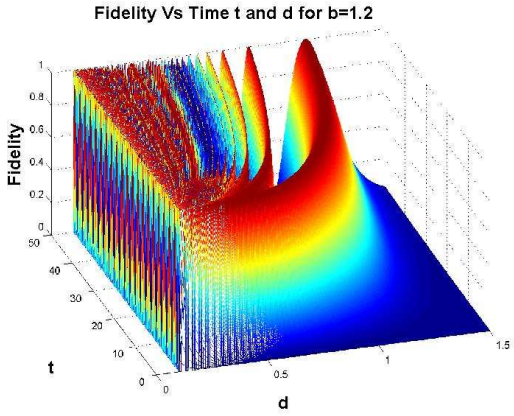

FIG. 19: Plot of Transfer Fidelity Versus Time and Interdot Distance ($b = 1.2$).

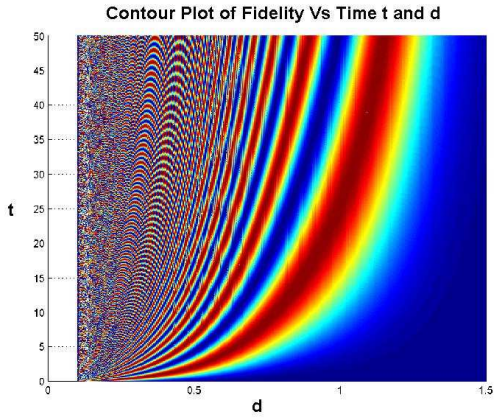

FIG. 20: Contour Plot of Transfer Fidelity Versus Time and Interdot Distance ($b = 1.2$).

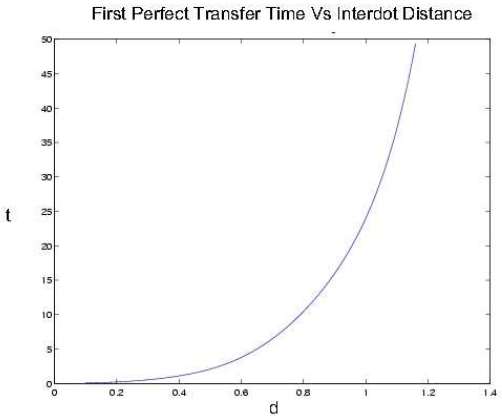

FIG. 21: Plot of time for first perfect transfer where fidelity $F = 1$. We observed that the optimum shortest transfer time is longer as d increases, indicating that the swapping between the quantum dots $\mathbf{S}_1$ and $\mathbf{S}_2$ is slower with larger interdot distance.

C. Decoherence in Quantum State Transfer

For real physical system, we see that the coupling of the quantum states to the environment leads to decoherence. We subject the system to the two decoherence models as described in the previous section, namely the depolarizing channel and dephasing channel. In the case of depolarizing channel, quantum dot system is subjected to interaction with the environment while it is evolving under the given Hamiltonian. By setting the initial state $\mathbf{S}_1$ such that $\alpha = \cos(\theta/2)$ and $\beta = \sin(\theta/2)$, we investigate the decoherence effect when noise admixture η is non-zero for different θ values. For the depolarizing channel, the transfer fidelity of the new states, which are now mixed states, are calculated using Eq. (**??**). Fig. (**??**) shows the maximum transfer fidelity value is smaller than unity when η is non-zero, implying that the perfect state transfer is no longer possible as long as noise is added to the system. We note that transfer fidelity does not appear to depend the initial state (i.e. the angle θ) but solely on the decoherence parameter η in the depolarizing channel. This may not be surprising in view of the isotropic nature of the model.

$$|\psi(t)\rangle = e^{-iHt}(|\psi\rangle|0\rangle) \tag{21}$$

$$\varrho_t = (1-\eta)|\psi(t)\rangle\langle\psi(t)| + \frac{\eta}{4}I_4 \tag{22}$$

$$\varrho_t^{red} = tr_1(\varrho_t). \tag{23}$$

$$F = tr(|\psi\rangle\langle\psi|\varrho_t^{red}) \tag{24}$$

For the second type of decoherence model, we apply dephasing channel to the quantum dot system shown in Eq. (**??**) where We note that the model acts on off-diagonal elements of the density matrix, which is not the case for decoherence under depolarizing channel. We again set $\gamma_A = \gamma_B = \gamma$ for the same reason. The transfer fidelities are then calculated using Eq. (**??**) after tracing out the first qubit. Fig. (**??**) shows how the average transfer fidelity changes as γ increases. Note that in this figure, the average transfer fidelity is unity only for $\gamma = 1$. The vertical bar at each γ value indicates the standard deviation of all transfer fidelities computed from randomly generated initial states $\mathbf{S}_1$, using differnt θ values, and the final state. Although a linear relation between the γ value and the average fidelity is observed in the same figure, the standard deviation is larger for smaller γ values.

$$\begin{aligned}\varrho_t &= \varepsilon_{AB}(|\psi(t)\rangle\langle\psi(t)|) \\ &= \begin{pmatrix} \rho_{11} & \gamma_B\rho_{12} & \gamma_A\rho_{13} & \gamma_A\gamma_B\rho_{14} \\ \gamma_B\rho_{21} & \rho_{22} & \gamma_A\gamma_B\rho_{23} & \gamma_A\rho_{24} \\ \gamma_A\rho_{31} & \gamma_A\gamma_B\rho_{32} & \rho_{33} & \gamma_B\rho_{34} \\ \gamma_A\gamma_B\rho_{41} & \gamma_A\rho_{42} & \gamma_B\rho_{43} & \rho_{44} \end{pmatrix}\end{aligned} \tag{25}$$

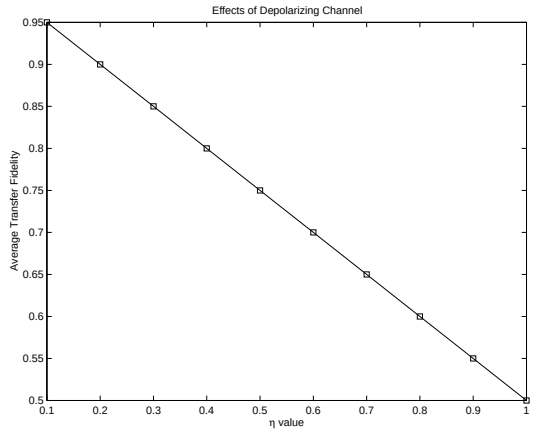

FIG. 22: Plot of transfer fidelity versus η under the influence of depolarizing channel. Note that the transfer fidelity decreases linearly as η increases.

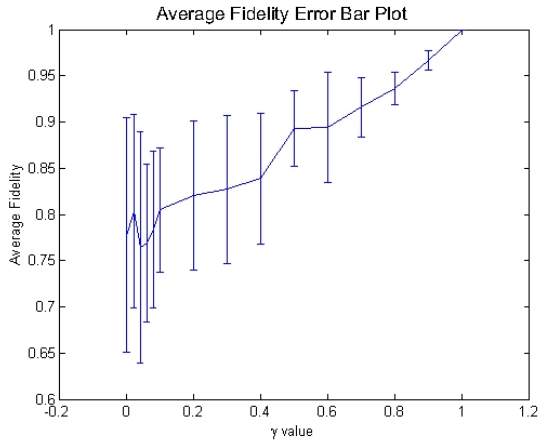

FIG. 23: Plot of transfer fidelity versus γ under the influence of dephasing channel. Note that the transfer fidelity is unity only at $\gamma = 1$.

V. CONCLUSION AND FINAL REMARKS

In this work, we have considered entanglement of formation for thermal states of two quantum dots subject to Heitler-London interaction. We explored how interdot distance and magnetic field affect the average fidelity for teleportation under different temperature and for state transfer. In the first part, we identify b, d and T values that provide good entanglement and produce better than classical fidelities for teleportation. We showed that the choice of such values reduces as the extent of decoherence increases, and in all cases, the average fidelity is always below unity. However, the process can still be achieved under moderate level of decoherence. In the second part, we showed that the system of quantum dots can achieve perfect state transfer or swap depending on the amount of the external magnetic field and the length of the interdot distance even under moderate noise or decay. In short, we see that quantum teleportation and quantum state transfer remains possible for a large range of magnetic field and interdot distance under decoherence.

G. Burkard, D. Loss, and D.P. DiVincenzo. *Phys. Rev. B* **59**, 2070 (1999)

G.Burkard, H.-A Engel, D. Loss, Fortschritte der Physik 48 9-11, 965-986 (2000).

A. C. Johnson, J. R. Petta, J. M. Taylor, A. Yacoby, M. D. Lukin, C. M. Marcus, M. P. Hanson and A. C. Gossard. *Nature* **435**, 925 (2005)

D. Loss, G. Burkard and E.V. Sukhorukov, Proceedings of the XXXIVth Rencontres de de Moriond "Quantum Physics at Mesoscopic Scale", Les Arcs, Savoie, France, January 23-30, 1999; quant-ph//9907133.

G. Burkard, D. Loss and E.V. Sukhorukov, Phys. Rev. B, **61** R16303 (2000).

G. Burkard and D. Loss, *Phys. Rev. B* **59** 2070 (1999).

J.A. Folk and C.M. Marcus, *Phys. Rev. Lett.* **87**, 206802 (2001).

M. Thorwart and Peter Hanggi, *Phys. Rev. A.* **65**, 012309 (2001).

T. Yu and J. H. Eberly, quant-ph/0305078.

C. H. Bennett, D. P. DiVincenzo, J. Smolin, and W. K. Wootters, *Phys. Rev. A* **54**, 3824 (1996).

C. H. Bennett, H. J. Bernstein, S. Popescu, and B. Schumacher, *Phys. Rev. A* **53**, 2046 (1996); S. Popescu, D. Rohrlich,"On the measure of entanglement for pure states," quant-ph/9610044.

J. J. Sakurai, Modern Quantum Mechanics, San Fu Tuan, ed. (jamin/Cummings, Menlo Park, CA, 1985), p. 277.

S. Hill and W. K. Wootters, *Phys. Rev. Lett.* **78**, 5022 (1997).

C. H. Bennett and S. J. Wiesner, *Phys. Rev. Lett.* **69**, 2881 (1992).

G. R. Guthörlein, M. Keller, K. Hayasaka, W. Lange, and H. Walther, *Nature* **414**, 49 (2001).

M. Christandl, N. Datta, A. Ekert, and A. J. Landahl, quant-ph/0309131.

M. Christandl, N. Datta, T. C. Dorlas, A. Ekert, A. Kay,

and A. J. Landahl, quant-ph/0411020.
V. Gorini, A. Kossakowski, and E.C.G. Sudarshan. Completely positive dynamical semigroups of n-level systems. Journal of Mathematical Physics, 17:821, 1976.
G. Lindblad. On the generators of quantum dynamical semigroups. Communications in Mathematical Physics, 48:119, 1976.